

Global Climate Pattern Behind Hydrological Extremes in Central India

Kironmala Chanda and Rajib Maity

Abstract The concurrent influence of large-scale, coupled oceanic–atmospheric circulation patterns was established to have an effect on hydrologic variability across the world. El Niño–Southern Oscillation (ENSO) and Indian Ocean Dipole (IOD) are, in particular, important for Indian hydroclimatology. However, it is now established that rather than just a few well-known teleconnection patterns, a Global Climate Pattern (GCP) comprising of a global field of several climate anomalies are responsible for above-normal and below-normal precipitation events over entire India. The existence of a GCP for hydrological extremes in an even smaller spatial scale is illustrated in this study. The central part of India, consisting of the contiguous homogeneous meteorological subdivisions—West Madhya Pradesh, East Madhya Pradesh, Vidarbha, and Chattisgarh (hereinafter ‘central India’), is selected as the study area. Hydrological extremes (this study focus on precipitation) in the study area are identified in terms of the Standardized Precipitation Anomaly Index (SPAI), which is suitable for quantifying extreme events in a monsoon-dominated climatology. After investigation of the global anomaly fields of five climate variables, a set of 19 specific zones of climate anomalies from across the world are found to constitute the GCP for the hydrological extremes in the study region. The identified GCP is further utilized in a Support Vector Machine (SVM) model to investigate the potential of the GCP in foreseeing dry and wet extremes over the study area.

K. Chanda

Indian Institute of Technology (Indian School of Mines), Dhanbad 826004, Jharkhand, India
e-mail: kironmala.iitkgp@gmail.com

R. Maity (✉)

Department of Civil Engineering, Indian Institute of Technology Kharagpur, Kharagpur
721302, West Bengal, India
e-mail: rajib@civil.iitkgp.ernet.in; rajibmaity@gmail.com

© Springer Nature Singapore Pte Ltd. 2018
V.P. Singh et al. (eds.), *Climate Change Impacts*, Water Science
and Technology Library 82, https://doi.org/10.1007/978-981-10-5714-4_6

71

Introduction

The association of large-scale atmospheric–oceanic circulation patterns and hydrologic variables across the world has been established through several studies. Recent studies have confirmed that asymmetry in the response of rainfall anomalies in different parts of the world result from opposite phases of low variability oceanic circulation patterns (King et al. 2013; Qiu et al. 2014). For example, observed changes in the frequency and intensity of precipitation extremes in Europe are now largely explained by the persistence in atmospheric circulation patterns over the North Atlantic (Willems 2013). Changes in large-scale circulation patterns are found to be responsible for the observed long-term warming and drying in central Europe (Philipp et al. 2007). For the past two decades, the role of specific oceanic–atmospheric circulation phenomenon such as, El Niño–Southern Oscillation (ENSO), Indian Ocean Dipole (IOD), Equatorial Indian Ocean Oscillation (EQUINOO), Pacific Decadal Oscillation (PDO), Atlantic Multi-decadal Oscillation (AMO), North Atlantic Oscillation (NAO) in triggering and enhancing droughts and floods on a continental scale have been the focus of research (Chiew and McMahon 2002; Terray et al. 2003; Gadgil et al. 2004; Goswami et al. 2006; Maity and Nagesh Kumar 2006, 2008; Feng and Hu 2008; Li et al. 2008; Mo and Schemm 2008; Ting et al. 2011; Singhrattna et al. 2012; Oubeidillah et al. 2012; Jiang et al. 2013; Rogers 2013; Wang et al. 2013). Some of the recent advances establish the influence of ENSO and AMO in relation to the variability of China’s summer precipitation (Gu et al. 2009; Ye 2014) as well as the frequency of its extreme precipitation events (Fu et al. 2013). The effect of NAO is found to affect winter precipitation, river flow, and temperature in the Mediterranean region (Brandimarte et al. 2011).

Some of the most frequently researched phenomena are ENSO and IOD, primarily because they influence rainfall anomalies in a large number of countries across the world. For instance, the unusual warming of the central and eastern tropical Pacific Ocean during the El Niño events is known to be responsible for below-normal precipitation in Indonesia and the surrounding Pacific islands and above-normal precipitation in the western coast of South America. The role of ENSO in biennial relationship of rainfall variability between Central and equatorial South America was also recently identified (Wu and Zhang 2010). In the Indian context, the occurrence of an El Niño event in the Pacific generally indicates that rainfall deficiencies are in the offing—dry and drought conditions may be expected due to poor Indian Summer Monsoon Rainfall (ISMR). However, the relationship between circulation patterns and the occurrence of anomalous continental scale hydrologic behavior is often very complicated. This is due to the possible involvement of a number of factors, some more rare than others, which lead to the optimum conditions for the development of an extreme hydrologic event. Thus, in a recent study, a direct relationship (as opposed to an inverse relationship) of ENSO with the rainfall and streamflow series in Mahanadi river basin of south India was observed (Panda et al. 2013). Again, some studies postulate that the ENSO-ISMR

relationship has weakened over the years (Viswambharan and Mohanakumar 2014). Apart from ENSO, the other most significant circulation pattern affecting ISMR is the IOD (Saji et al. 1999; Webster et al. 1999). A positive IOD event, which is accompanied by high SST over the western Indian Ocean, is known to affect ISMR positively with abundant rainfall in the Indian subcontinent and dry and drought conditions in Australia and Indonesia.

Existing literature indicates that most of the previous studies had investigated the role of specific large-scale Oceanic–Atmospheric Circulation Patterns (OACPs) in causing extreme hydrologic events such as droughts and floods. However, it is now established that apart from the well-known teleconnection patterns such as ENSO, IOD, etc., the concurrent effect of global anomaly fields of several climate variables influences hydrologic events in a regional scale (Chanda and Maity 2016). Considering the entire Indian landmass (also referred as all-India) as the test bed, it was demonstrated that a distinct Global Climate Pattern (GCP) consisting of 15 climate anomaly zones is responsible for the occurrence of dry and wet events. The potential of the GCP in predicting dry and wet events on an all-India scale is also established. In fact, the GCP is found to be more useful as precursor of hydrologic extremes in India compared to the most commonly used hydroclimatic teleconnection patterns in the Indian context. The objective of this study is to explore the existence of a distinct GCP for hydrologic events on a smaller spatial scale. Central India is selected as the target area to explore the association of regional dry/wet events with global anomaly fields of five climate variables—sea surface temperature, surface pressure, air temperature, wind speed, and total precipitable water. The specific GCP for central India, once identified, is utilized as an input to a prediction model for categorizing hydrologic events into dry, normal, and wet. Based on experience from the previous study, a temporal scale of three months is adopted for this study as the climate anomaly zones are found to be sufficiently well-defined at this scale for identification of GCP.

Study Area and Data

The India Meteorological Department (IMD) divides India into 36 homogenous meteorological subdivisions. Out of these, four contiguous subdivisions, namely, West Madhya Pradesh, East Madhya Pradesh, Vidarbha, and Chattisgarh are considered together as the study area (Fig. 1). The study area is referred as ‘central India’. The monthly precipitation data of the aforementioned four subdivisions are obtained from IMD for the period 1959–2010. The datasets are downloaded from the website of Indian Institute of Tropical Meteorology (IITM) (<ftp://www.tropmet.res.in/pub/data/rain/iitm-regionrf.txt>). The method of development of the dataset along with the information of the raingauge distribution may be found in Parthasarathy et al. (1995), Rajeevan et al. (2006). The climate variables used for this study are the global fields of Sea Surface Temperature (SST), Surface Pressure (SP), Air Temperature (AT), Wind Speed (WS), and Total Precipitable Water

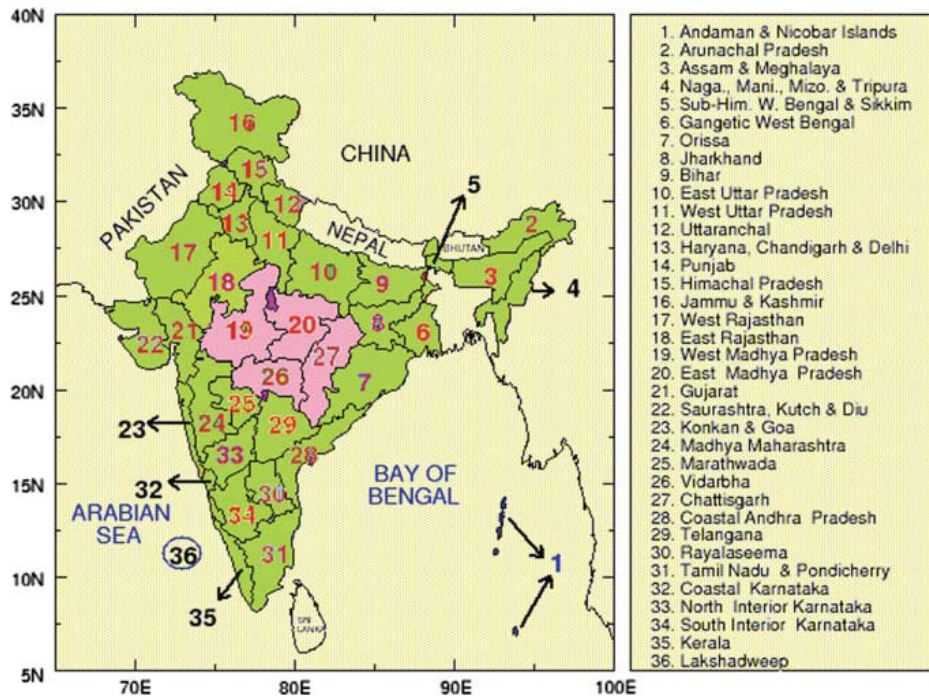


Fig. 1 Study area consisting of the four contiguous homogeneous meteorological Sub divisions of India—West Madhya Pradesh, East Madhya Pradesh, Vidarbha, and Chattisgarh (modified from map provided by Indian Institute of Tropical Meteorology, Pune, web address: www.tropmet.res.in)

(TPW). Monthly global gridded datasets of these variables are obtained from National Oceanic and Atmospheric Administration (NOAA) (<http://www.esrl.noaa.gov/psd/data/gridded/data.ncep.reanalysis.surface.html>) for the period 1958–2010. The spatial resolution of AT, SP, WS and TPW data is $2.5^\circ \text{ lat} \times 2.5^\circ \text{ lon}$ and that of SST data is of $2^\circ \text{ lat} \times 2^\circ \text{ lon}$.

Methodology

Quantification of Dry and Wet Events Through Standardized Precipitation Anomaly Index (SPAI)

Since the study area (i.e., central India) encompasses of the four aforementioned meteorological subdivisions, the monthly rainfall of these four meteorological subdivisions is averaged to get the monthly time series rainfall over the study area. In order to identify the GCP for dry and wet extremes, the time series of Standardized Precipitation Anomaly Index (SPAI) is computed from the obtained

precipitation time series. Details of the anomaly-based SPAI can be found in Chanda and Maity (2015). The SPAI is established to be a generalized index that is suitable for the characterization of meteorological droughts in monsoon-dominated climatology such as India (Chanda and Maity 2015). A temporal scale of three months is used for SPAI computation and the period 1961–1990 is used to represent the long-term climatology, based on which the rainfall anomalies are calculated. Following the guideline of the U.S. Drought Monitor regarding the threshold value of Standardized Precipitation Index (SPI) indicating drought, the criteria adopted for this study are: SPAI-3 values less than -0.8 are designated as *dry* events, those greater than 0.8 are designated as *wet* events and those in between are designated as *normal* events.

Identification of the Global Climate Pattern (GCP) for Central India

Since a temporal scale of 3 months is used for identifying the dry and wet events, the global climate anomaly fields are also considered at a temporal scale of three months. For each dry event (i.e., $\text{SPAI-3} < -0.8$), the climate anomaly field at the preceding 3-month period is considered. For instance, for a dry event comprising the months April–May–June, the global climate anomaly field is obtained from the period January–February–March. For each of the climate variables, the global anomaly field corresponding to all observed dry events during the period 1959–2000 is obtained and they are averaged event-wise to get the mean global gridded climate anomaly field for dry events (Chanda and Maity 2016). A similar procedure is followed to get the mean global gridded climate anomaly field for wet events for each climate variable. For a given climate variable, the grid-wise difference of anomalies between dry and wet events is computed and maps showing the anomaly differences are plotted. On inspection of these maps, it is found that contrasting (above-normal/below-normal) features of climate anomalies are revealed during dry and wet events at the target location. A particular zone on the globe consisting of opposite anomalies of a climate variable corresponding to dry and wet events at the study area is considered as one of the variables constituting the GCP. All such variables, together forming the GCP, are used as input to a prediction model for categorizing dry and wet events.

Utilization of the Identified GCP for Prediction of Dry and Wet Events in Central India

The potential of the GCP in prediction of dry and wet events in India has been recently established (Chanda and Maity 2016). In this study, a smaller target area,

i.e., central India has been selected and the GCP responsible for dry and wet extremes in this region is investigated. The potential of the identified GCP for prediction of hydrologic extremes in central India is assessed through the following steps.

Reduction of Dimensionality of GCP

Since the curse of dimensionality of inputs could affect the prediction process, it is wise to reduce the large number of variables constituting the GCP. However, the information contained in the identified inputs must not be lost in the process. Hence, principal component analysis (PCA) (Jolliffe 1986) is used to orthogonally transform the dataset from a number of observed correlated variables to a number of uncorrelated components which explain the variance of the target variable in a gradually decreasing order. The number of principal components considered should be such that it should be large enough to substantially explain the variability. However, it should not be too large so as to hamper the SVM training owing to high dimensionality.

Model for Classification of Dry and Wet Events

Once a number of principal components of the GCP are identified as inputs, the next step is to devise a prediction model that can classify the events into different categories. The three categories that are considered in this study are *dry* ($SPAI < -0.8$), *normal* ($-0.8 \leq SPAI \leq 0.8$) and *wet* ($SPAI > 0.8$), respectively. It is true that sometimes more number of categories, indicating different levels of severities of dry and wet events, are of interest. However, any finer categorization is avoided here since the observed number of events in each category would then become too less to train the prediction model as well as to evaluate the prediction performance. Support Vector Machines (SVM) are one of the machine learning techniques that classify data points using a hypothesis space of linear functions in a high-dimensional feature space. It maps the input space to a higher dimensional feature space and selects a hyperplane to attain maximum separation between the different classes. SVMs have been successfully used in hydrological applications (Bray and Han 2004; Qin et al. 2005; She and Basketfield 2005; Tripathi et al. 2006; Lin et al. 2006; Anirudh and Umesh 2007; Kişi and Çimen 2009; Chen et al. 2010; Maity et al. 2010; Samsudin et al. 2011; Bhagwat and Maity 2012; Zakaria and Shabri 2012; Raghavendra and Deka 2014). SVM-based models may be suitably used in classifying dry, normal and wet events based on the selected components (Chanda and Maity 2016).

Following Chanda and Maity (2016), two SVM models (named SVM-I and SVM-II) are used simultaneously to process the inputs, i.e., the selected principal

components. SVM-I performs classification into two categories—*dry* ($SPAI < -0.8$) and *not dry* ($SPAI \geq -0.8$), while SVM-II performs classification into two categories—*not wet* ($SPAI \leq 0.8$) and *wet* ($SPAI > 0.8$). After training the two SVM models during the model development period (1959–2000), they are used for classification for both model development (1959–2000) and testing period (2001–2010). At any given time step, the output from the two SVM models is logically joined to obtain the final output. When the output of SVM-I is dry and that of SVM-II is not wet, then the event is categorized as dry. When the output of SVM-I is not dry and that of SVM-II is wet, then the event is categorized as wet. When the outputs of SVM-I and SVM-II are not dry and not wet, respectively, the event is categorized as normal. If the outputs of the two SVM models are contradictory, i.e., SVM-I classifies the event as dry and SVM-II classifies it as wet, then the model fails to categorize the event. However, these events are also categorized into normal to prevent loss of data during evaluation of prediction performance, which is a little deviation from Chanda and Maity (2016). The categorization procedure is illustrated with the help of a flowchart (Fig. 2). It may be noted that three-way classification (say, groups A, B, and C) through SVMs is also possible. However, in such cases, two steps need to be followed. First, the classification has to be performed between ‘Group A’ versus ‘Group B and Group C’. In the next step, the candidates falling in the second category may be classified further into ‘Group B’ and ‘Group C’. For such classification, training the SVM becomes computationally too intensive. Thus, in this study, two separate SVM models for bi-category classification are used simultaneously and their outputs are logically joined to obtain a three-way classification.

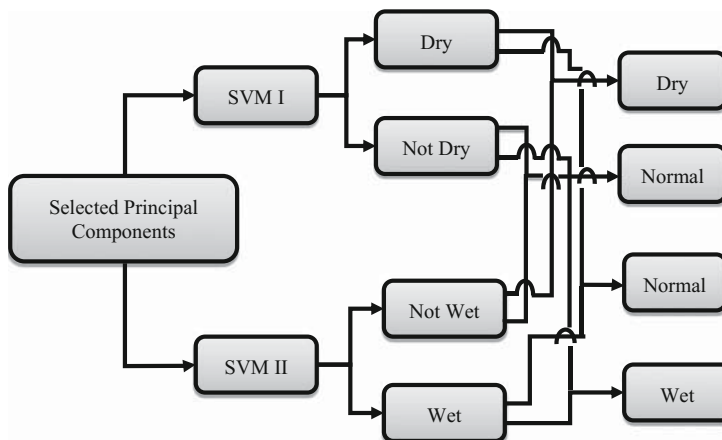


Fig. 2 Flowchart showing logical combination of the outputs of two SVMs to obtain final categorization of hydrological events

Evaluation of the Prediction Performance Using GCP as Input

After obtaining the final output obtained from the logical combination of the two SVM models, the prediction performance may be evaluated by constructing a contingency table for both the development and the testing period. The potential of classification of dry, normal, and wet events in the target area using the GCP as input may be assessed by inspecting the number of events (in the three-way contingency table) which are categorized correctly. Quantitatively, the model performance may be assessed in terms of Contingency Coefficient (C) (Pearson 1904), which is used to measure the degree of association in a contingency table for N samples (Gibbons and Chakraborti 2011). It is expressed as

$$C = \sqrt{\frac{Q}{Q+N}}, \quad (1)$$

where Q is a statistic that tests the null hypothesis that there is no association between the observed and predicted categories. Q is expressed as

$$Q = \sum_{i=1}^m \sum_{j=1}^n \frac{(NX_{ij} - X_i Y_j)^2}{NX_i Y_j}, \quad (2)$$

where X_{ij} is the number of cases falling in i th observed and j th predicted category, m and n are the number of observed and predicted categories respectively, and $X_i = \sum_{j=1}^n X_{ij}$ and $Y_j = \sum_{i=1}^m Y_{ij}$. The statistics Q approximately follows chi-square distribution with $\nu = (m-1)(n-1)$ degrees of freedom. The null hypothesis (no association between observed and predicted categories) may be rejected if the p -value is very low. The higher the value of C , the better the association between observed and predicted categories. The maximum value of C is theoretically 1, but its upper bound is given by

$$C_{\max} = \sqrt{\frac{t-1}{t}}, \quad (3)$$

where $t = \min(m, n)$ (Gibbons and Chakraborti 2011). The C value as well as the ratio C/C_{\max} may be used as a measure of the degree of association (Maity et al. 2013).

Results and Discussions

Identification of the Global Climate Pattern for Central India

The SPAI values computed from the trimonthly rainfall series of central India are used to categorize each time step in the development (1959–2000) and testing period (2001–2010) as dry, normal and wet event. During the development period, the number of dry, normal and wet events are found to be 90, 308, and 106 respectively. During the testing period, the same is found to be 27, 72, and 21 respectively.

As mentioned earlier, for each of the climate variables (SST, SP, AT, WS, TPW), the global anomaly field corresponding to all observed dry events during the period 1959–2000 is obtained and they are averaged event-wise to get the mean global gridded climate anomaly field for dry events. Following a similar procedure, the mean global gridded climate anomaly field for wet events is also obtained for each variable. The grid-wise anomaly difference maps are subsequently investigated for identifying the zones with contrasting anomaly features during dry and wet events. For many grid locations, the difference in anomalies is found to be statistically significant at 99% confidence level. From the large contiguous zones of statistically significant anomaly differences, the core areas are selected as constituent variables forming the GCP. In all, the GCP for central India is characterized by 19 globally distributed zones from five climate variables. The spatial location and extent of the zones are discussed in comparison to those identified in case of ‘all-India’ analysis (Chanda and Maity 2016) in the following subsections.

Global Fields of Sea Surface Temperature (SST)

Figure 3a reproduces the SST anomaly difference map for ‘all-India’ analysis from Chanda and Maity (2016). For dry and wet extremes in central India, which is the target area for this study, the global SST anomaly difference map is shown in Fig. 3b.

The large positive anomaly zone (5°N – 5°S and 100°W – 140°W) in the equatorial Pacific Ocean is evident in the case of all-India analysis as well as ‘central India’ analysis. However, for central India, this zone is not as strong as in the case of the SST patterns for all-India. The lessening of this zone in extent as well as magnitude may be indicative of the fact that the effect of El Niño on dry and wet extremes in central India are weaker than the same on dry and wet extremes occurring on all-India scale. In both Fig. 3a, b, the positive anomaly differences in northern Pacific Ocean (40°N – 48°N and 150°W – 165°W) are even stronger than those in the equatorial region. The two negative anomaly zones in the Pacific (20°S – 26°S and 160°E – 170°E ; 40°S – 50°S , 114°W – 124°W) are found to be potent in both Fig. 3a, b. However, the negative anomaly region (26°N – 34°N , 136°E – 144°E) along the

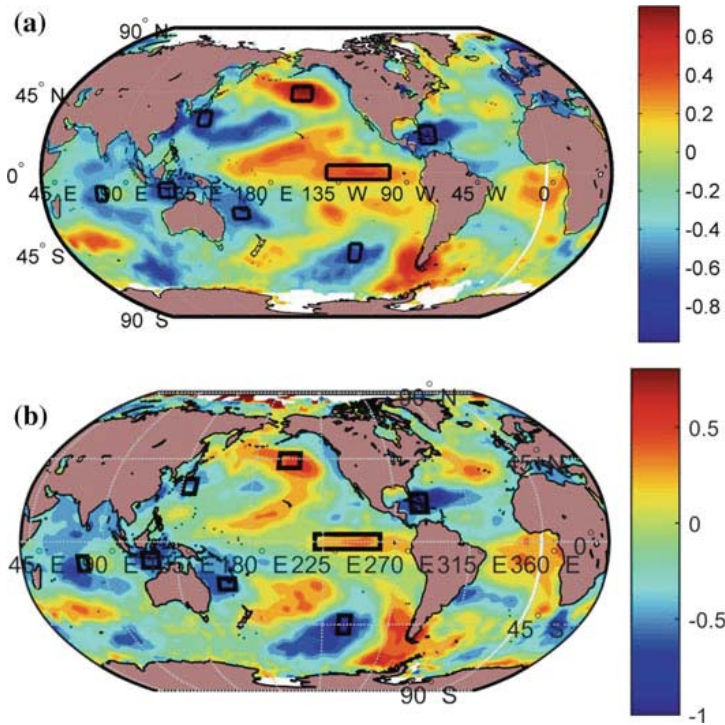


Fig. 3 Differences in mean SST anomalies during dry events (SPAI-3 < -0.8) and wet events (SPAI-3 > 0.8) over **a** India (Chanda and Maity 2016) and **b** central India

coast of Japan is found to be relatively less well defined in case of central India (Fig. 3b). In general, it is observed that warm anomaly pockets in the eastern part of Pacific Ocean and cold anomaly pockets in the western part of Pacific Ocean are associated with dry events in central India as well as ‘all-India’.

As in case of the SST over Pacific Ocean, the negative anomaly regions in sub-equatorial Indian Ocean (8°S–16°S and 74°E–80°E) and to the west of Australia (6°S–14°S and 114°E–124°E) are similar in extent and magnitude in Fig. 3a, b. The strong negative anomaly region (16°N–26°N and 70°W–80°W) between the North and South Americas is also equally well defined in both the figures.

Thus, it may be concluded that the global SST zones responsible for dry and wet extremes in central India are identical to those of all-India. Hence, 8 SST zones are selected as constituents of the GCP for central India.

Global Fields of Surface Pressure (SP)

Figure 4a reproduces the SP anomaly difference map for ‘all-India’ analysis from Chanda and Maity (2016). For dry and wet extremes in central India, the global SP anomaly difference map is shown in Fig. 4b. The positive anomaly zone in northern Pacific (55°N–65°N and 145°W–160°W) as well as the negative anomaly zone in tropical Pacific (15°N–30°N, 145°W–160°W) is found to be very well defined and strong for both ‘all-India’ and central India. In addition to these two regions in Pacific Ocean, a very prominent positive anomaly zone in the western part of equatorial Pacific (5°S–5°N, 170°E–210°E) is observed in case of central India. The whole of Arabian Sea, Indian Ocean, and Bay of Bengal exhibit positive anomalies in both Fig. 4a, b. The signature of this region is represented through the zone 10° N–20°N, 55°E–65°E. The mild negative anomaly region in the Atlantic is also similar in extent and magnitude in both the figures. Thus, a total of 5 SP zones is selected as constituents of the GCP for central India.

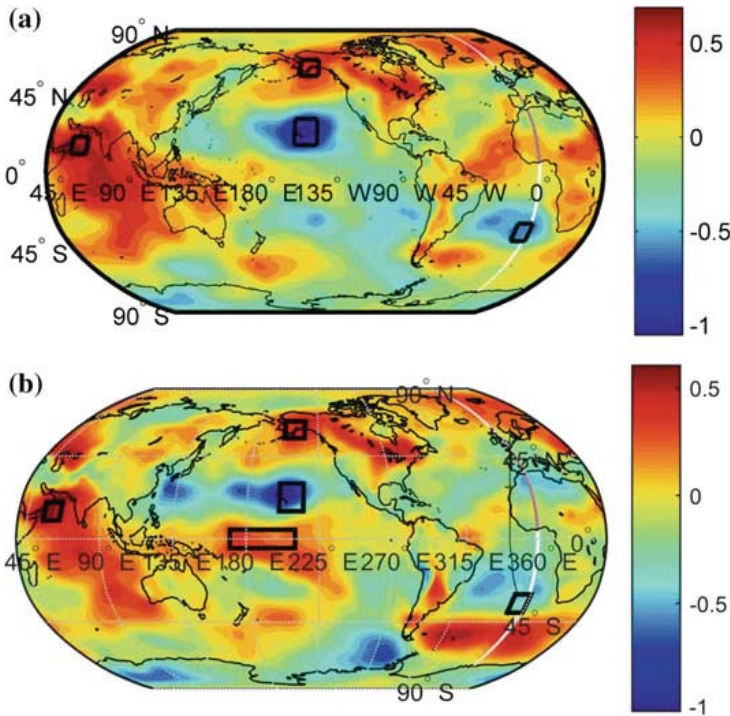


Fig. 4 Differences in mean SP anomalies during dry and wet events in **a** India (Chanda and Maity 2016) and **b** central India

Global Fields of Air Temperature (AT), Wind Speed (WS), and Total Precipitable Water (TPW)

Since the variables AT, WS, and TPW generally influence convective activity on a smaller spatial scale, the anomaly fields of these variables are investigated around the Indian subcontinent region. The patterns of anomaly differences of AT during dry and wet events in case of ‘all-India’ and in case of ‘central India’ are shown in Fig. 5a, b, respectively. Similar comparative figures for WS and TPW are shown in Figs. 6a, b and 7a, b, respectively. In case of AT, it is observed that a positive anomaly region at the nook of the Bay of Bengal is associated with dry events for all-India as well as for central India. For central India, a negative anomaly zone below the landmass of Pakistan and Iran is also found to be very much prominent in extent and magnitude, much more than that observed in case of the all-India study. Hence, both the AT zones—(20°N–30°N and 85°E–95°E) and (20°N–25°N and 60°E–65°E) are considered in the pool of GCP for central India.

Positive WS anomalies in the Indian Ocean are found to be associated with dry events in all-India as well as central India. As observed in case of AT, here also, a zone of importance can be located over the landmass of Pakistan and Iran. This positive anomaly region was evident in case of ‘all-India’ also, but the magnitude of the anomaly was not as large as in the present case. As a result, two WS zones—(0°–5°N, 70°E–85°E) and (25°N–30°N, 60°E–70°E) are considered while developing the GCP for central India.

Very strong negative TPW anomalies around the Persian Gulf are found to be associated with dry events in ‘India’ as well as ‘central India’. Additionally, a positive anomaly zone located to the west of Pakistan is also found to be very prominent in case of central India. The hint of this zone was evident in case of

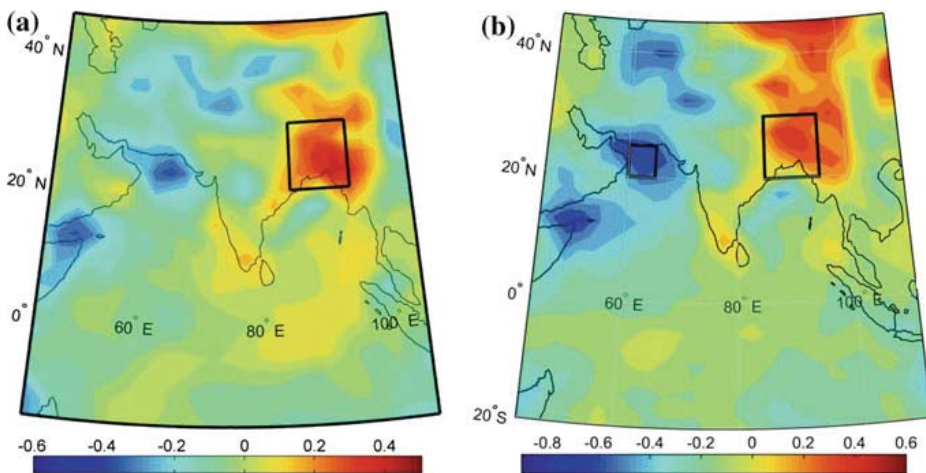


Fig. 5 Differences in mean AT anomalies during dry and wet events in **a** India (Chanda and Maity 2016) and **b** central India

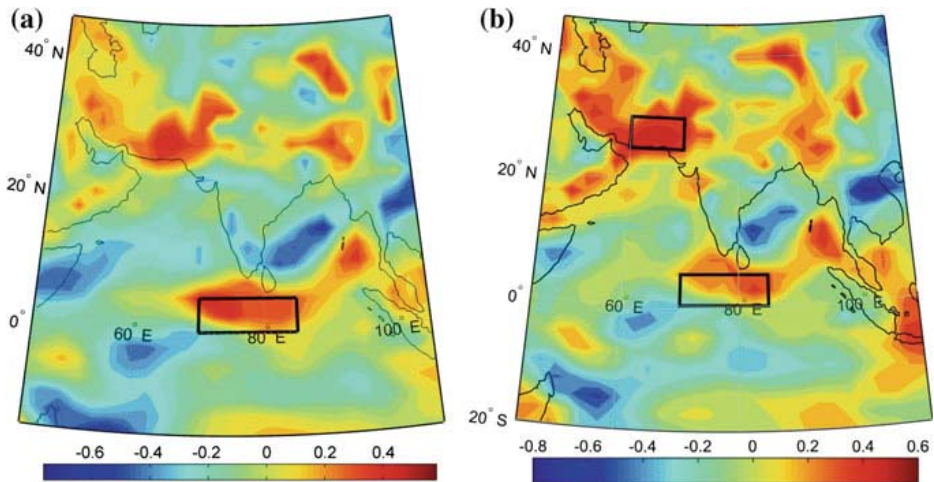


Fig. 6 Differences in mean WS anomalies during dry and wet events in **a** India (Chanda and Maity 2016) and **b** central India

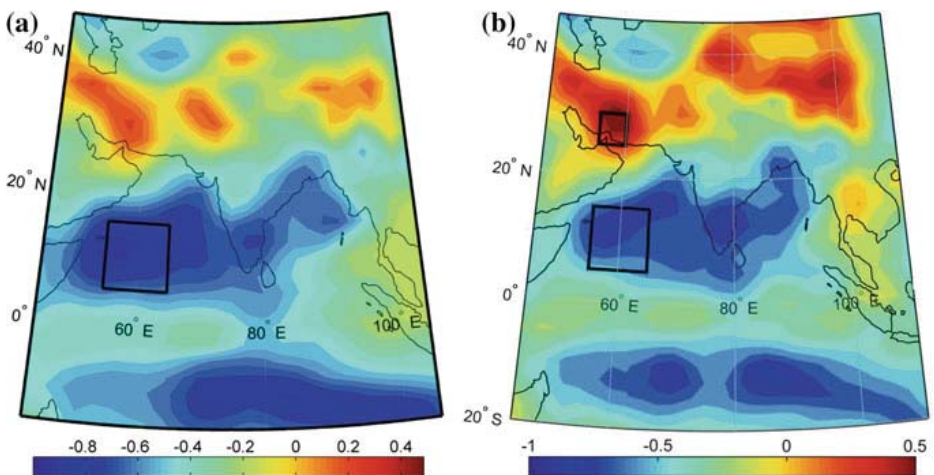


Fig. 7 Differences in mean TPW anomalies during dry and wet events in **a** India (Chanda and Maity 2016) and **b** central India

all-India study also, but was not as well defined. Thus, TPW zones—(5°N–15°N and 55°E–65°E) and (25°N–30°N and 55°E–60°E) are considered for central India.

Thus, in all, a total of 19 variables, each being denoted by a specific climate anomaly from a distinct part of the globe, together constitutes the GCP for dry and wet events in central India. The extent of these zones is specifically mentioned in Table 1. It is observed that many of the variables are equally important factors affecting hydrologic extremes in the ‘central India’ region as well as on an ‘all-India’ scale. However, it is noted that often the extent of the anomaly zones as well as their magnitudes differ in case of the present study concerning central India

Table 1 Identified representative zones of climate anomalies to characterize the global climate pattern (GCP) responsible for hydrologic extremes in central India

Physical variable	Symbol	Latitude	Longitude
Air temperature	AT1	20°N–30°N	85°E–95°E
Air temperature	AT2	20°N–25°N	60°E–65°E
Wind speed	WS1	0°N–5°N	70°E–85°E
Wind speed	WS2	25°N–30°N	60°E–70°E
Total precipitable water	TPW1	5°N–15°N	55°E–65°E
Total precipitable water	TPW2	25°N–30°N	55°E–60°E
Surface pressure	SP1	15°N–30°N	145°W–160°W
Surface pressure	SP2	30°S–40°S	0°W–10°W
Surface pressure	SP3	55°N–65°N	145°W–160°W
Surface pressure	SP4	10°N–20°N	55°E–65°E
Surface pressure	SP5	5°S–5°N	170°E–210°E
Sea surface temperature	SST1	40°N–48°N	150°W and 164°W
Sea surface temperature	SST2	16°N–26°N	70°W–80°W
Sea surface temperature	SST3	20°S–26°S	160°E–170°E
Sea surface temperature	SST4	4°N and 4°S	100°W and 140°W
Sea surface temperature	SST5	8°S and 16°S	74°E and 80°E
Sea surface temperature	SST6	6°S–14°S	114°E–124°E
Sea surface temperature	SST7	40°S–50°S	116°W–124°W
Sea surface temperature	SST8	26°N–34°N	136°E–144°E

and the all-India study. Moreover, some local factors (such AT, WS and TPW) which have limited influence on the hydrologic extremes of India are found to be more influential in case of central India.

Utilization of the Identified GCP for Prediction of Dry and Wet Events in Central India

As mentioned earlier, the number of principal components selected should substantially explain the variability and also alleviate the curse of dimensionality. It is found that the first seven principal components together explain about 72.5% of the variability. Hence, the seven selected principal components of the 19-dimensional GCP for the model development period are used as inputs to train the two SVM models. The models are then used for classification of the events at each time step (both development and testing period) into dry, normal, or wet category. The prediction performance is subsequently assessed by inspecting the contingency table (Table 2). During the development period, 59 out of the 90 observed dry events are correctly predicted while 12 and 19 observed droughts are wrongly predicted as normal and wet respectively. Of the 106 observed wet events, 60 are

Table 2 Contingency table for multiclass classification using identified GCP for central India

Performance assessment criteria/statistics	Model performance										
	Development period (1959–2000)					Testing period (2001–2010)					
	Observed category	Predicted category			Observed category	Predicted category					
		Dry	Normal	Wet		Dry	Normal	Wet	Dry	Normal	Wet
	59	12	19	11	8	8	11	8	8		
	105	77	126	9	14	49	9	14	49		
	30	16	60	2	2	17	2	2	17		
Q	43.29										
ν	4										
p value	8.9×10^{-9}										
C	0.281										
C_{\max}	0.707										
C/C_{\max}	0.398										
						18.27					
						4					
						0.0011					
						0.364					
						0.707					
						0.515					

correctly predicted while 30 and 16 observed wet events are wrongly predicted as dry and normal, respectively. During the testing period, the number of observed dry events predicted correctly is 11 (out of a total of 27) and the number of observed wet events predicted correctly is 17 (out of a total of 21). The value of the Contingency Coefficient C is obtained as 0.281 and 0.364 during the development and testing period respectively. The low p -values and reasonably good C/C_{\max} ratios indicate a good performance considering that prediction of regional hydrological extremes is immensely complicated due to large uncertainty in the climatic system. Thus, it is observed that GCP identified for hydrological extremes in central India may serve as effective precursors of dry and wet events.

Conclusion

This study reinforces the fact that hydrological extremes at the regional scale are caused by the concurrent effect of several climate anomaly fields across the globe rather than only well-known atmospheric–oceanic circulation patterns. A total of 19 globally distributed anomaly zones of different climate variables are found to constitute the Global Climate Pattern (GCP) responsible for hydrological extremes in central India. For the large-scale variables such as sea surface temperature and pressure, the zones of importance for central India are more or less similar to that of all India. However, for variables like air temperature, wind speed and total precipitable water, the number of influential zones is found to be more in number and relatively better defined for central India than that in case of all-India.

The identified GCP for central India is found to have potential use as precursor of hydrologic extremes in the target area. The SVM-based modeling approach used in this study exhibits reasonably good potential of GCP in foreseeing the above-and below-normal precipitation events. It may be possible to obtain more reliable prediction using GCP by adopting further sophisticated modeling approach. Moreover, as a future extension of this work, the illustrated methodology may be applied for other homogeneous meteorological subdivisions of India having considerably different precipitation regime.

Acknowledgements This study is partially supported by the Ministry of Earth Science (MoES), Government of India, through sponsored Project No. MoES/PAMC/H&C/30/2013-PC-II.

References

- Anirudh V, Umes CK (2007) Classification of rainy days using SVM. In: Proceedings of Symposium at HYDRO, Norfolk, Virginia, USA
- Bhagwat PP, Maity R (2012) Multistep-ahead river flow prediction using LS-SVR at daily scale. *J Water Resour Prot* 4:528–539. doi:[10.4236/jwarp.2012.47062](https://doi.org/10.4236/jwarp.2012.47062)

- Brandimarte L, Di Baldassarre G, Bruni G, D'Odorico P, Montanari A (2011) Relation between the north-atlantic oscillation and hydroclimatic conditions in mediterranean areas. *Water Resour Manag* 25(5):1269–1279
- Bray M, Han D (2004) Identification of support vector machines for runoff modelling. *J Hydroinform* 6:265–280
- Chanda K, Maity R (2015) Meteorological drought quantification with standardized precipitation anomaly index (SPAI) for the regions with strongly seasonal and periodic precipitation. *J Hydrol Eng ASCE* 06015007-1–06015007-7. doi:[10.1061/\(ASCE\)HE.1943-5584.0001236](https://doi.org/10.1061/(ASCE)HE.1943-5584.0001236)
- Chanda K, Maity R (2016) Uncovering global climate fields causing local precipitation extremes. *Hydrol Sci J*. doi:[10.1080/02626667.2015.1006232](https://doi.org/10.1080/02626667.2015.1006232) (Taylor and Francis)
- Chen H, Guo J, Wei X (2010) Downscaling GCMs using the smooth support vector machine method to predict daily precipitation in the Hanjiang basin. *Adv Atmos Sci* 27(2):274–284. doi:[10.1007/s00376-009-8071-1](https://doi.org/10.1007/s00376-009-8071-1)
- Chiew FHS, McMahon TA (2002) Global ENSO-streamflow teleconnection, streamflow forecasting and interannual variability. *Hydrol Sci J* 47(3):505–522
- Feng S, Hu Q (2008) How the North Atlantic multidecadal oscillation may have influenced the Indian summer monsoon during the past two millennia. *Geophys Res Lett* 35:L01707. doi:[10.1029/2007GL032484](https://doi.org/10.1029/2007GL032484)
- Fu G, Yu J, Yu X, Ouyang R, Zhang Y, Wang P, Liu W, Min L (2013) Temporal variation of extreme rainfall events in China, 1961–2009. *J Hydrol*. doi:[10.1016/j.jhydrol.2013.02.021](https://doi.org/10.1016/j.jhydrol.2013.02.021)
- Gadgil S, Vinayachandran PN, Francis PA, Gadgil S (2004) Extremes of the Indian summer monsoon rainfall, ENSO and equatorial Indian Ocean oscillation. *Geophys Res Lett* 31:L12213. doi:[10.1029/2004GL019733](https://doi.org/10.1029/2004GL019733)
- Gibbons JD, Chakraborti S (2011) *Nonparametric statistical inference*, 5th edn. Chapman and Hall, Boca Raton
- Goswami BN, Madhusoodanan MS, Neema CP, Sengupta D (2006) A physical mechanism for North Atlantic SST influence on the Indian summer monsoon. *Geophys Res Lett* 33:L02706. doi:[10.1029/2005GL024803](https://doi.org/10.1029/2005GL024803)
- Gu W, Li C, Li W, Zhou W, Chan JCL (2009) Interdecadal unstationary relationship between NAO and east China's summer precipitation patterns. *Geophys Res Lett* 36:L13702. doi:[10.1029/2009GL038843](https://doi.org/10.1029/2009GL038843)
- Jiang P, Gautam M, Zhu J, Yu Z (2013) How well do the GCMs/RCMs capture the multi-scale temporal variability of precipitation in the Southwestern United States? *J Hydrol* 479:75–85. doi:[10.1016/j.jhydrol.2012.11.041](https://doi.org/10.1016/j.jhydrol.2012.11.041)
- Jolliffe IT (1986) *Principal component analysis*. Springer, New York
- King AD, Alexander LV, Donat MG (2013) Asymmetry in the response of eastern Australia extreme rainfall to low-frequency Pacific variability. *Geophys Res Lett* 40:2271–2277. doi:[10.1002/grl.50427](https://doi.org/10.1002/grl.50427)
- Kişi O, Çimen M (2009) Evapotranspiration modelling using support vector machines. *Hydrol Sci J* 54(5):918–928
- Li S, Perlwitz J, Quan X, Hoerling MP (2008) Modelling the influence of North Atlantic multidecadal warmth on the Indian summer rainfall. *Geophys Res Lett* 35:L05804. doi:[10.1029/2007GL032901](https://doi.org/10.1029/2007GL032901)
- Lin J-Y, Cheng C-T, Chau K-W (2006) Using support vector machines for long-term discharge prediction. *Hydrol Sci J* 51(4):599–612
- Maity R, Nagesh Kumar D (2006) Hydroclimatic association of the monthly summer monsoon rainfall over India with large-scale atmospheric circulations from tropical Pacific Ocean and the Indian Ocean region. *Atmos Sci Lett* 7:101–107. doi:[10.1002/asl.141\(RMetS\)](https://doi.org/10.1002/asl.141(RMetS))
- Maity R, Nagesh Kumar D (2008) Basin-scale stream-flow forecasting using the information of large-scale atmospheric circulation phenomena. *Hydrol Process* 22(5):643–650. doi:[10.1002/hyp.6630](https://doi.org/10.1002/hyp.6630)
- Maity R, Bhagwat PP, Bhatnagar A (2010) Potential of support vector regression for prediction of monthly streamflow using endogenous property. *Hydrol Process* 24:917–923. doi:[10.1002/hyp.7535](https://doi.org/10.1002/hyp.7535)

- Maity R, Ramadas M, Govindaraju RS (2013) Identification of hydrologic drought triggers from hydro-climatic predictor variables. *Water Resour Res Am Geophys Union* 49(7):4476–4492. doi:[10.1002/wrcr.20346](https://doi.org/10.1002/wrcr.20346)
- Mo KC, Schemm JE (2008) Relationships between ENSO and drought over the southeastern United States. *Geophys Res Lett* 35:L15701. doi:[10.1029/2008GL034656](https://doi.org/10.1029/2008GL034656)
- Oubeidillah AA, Tootle G, Anderson S-R (2012) Atlantic Ocean sea-surface temperatures and regional streamflow variability in the Adour-Garonne basin, France. *Hydrol Sci J* 57(3):496–506
- Panda DK, Kumar K, Ghosh S, Mohanty RK (2013) Streamflow trends in the Mahanadi River basin (India): linkages to tropical climate variability. *J Hydrol*. doi:[10.1016/j.jhydrol.2013.04.054](https://doi.org/10.1016/j.jhydrol.2013.04.054)
- Parthasarathy B, Munot AA, Kothaale DR (1995) All-India monthly and seasonal rainfall series: 1871–1993. *Theor Appl Climatol* 49:217–224
- Pearson K (1904) On the theory of contingency and its relation to association and normal correlation. *Draper's Comp Res Mem Biometric Ser I*, Dulau and Co., London, U.K
- Philipp A, Della-Marta PM, Jacobeit J, Fereday DR, Jones PD, Moberg A, Wanner H (2007) Long-term variability of daily North Atlantic-European pressure patterns since 1850 classified by simulated annealing clustering. *J Clim* 20:4065–4095
- Qin Z, Yu Q, Li J, Wu Z, Hu B (2005) Application of least squares vector machines in modelling water vapor and carbon dioxide fluxes over a cropland. *J Zhejiang Univ Sci B* 6(6):491–495. doi:[10.1631/jzus.2005.B0491](https://doi.org/10.1631/jzus.2005.B0491)
- Qiu Y, Cai W, Guo X, Ng B (2014) The asymmetric influence of the positive and negative IOD events on China's rainfall. *Sci Rep* 4:4943. doi:[10.1038/srep04943](https://doi.org/10.1038/srep04943)
- Raghavendra NS, Deka PC (2014) Support vector machine applications in the field of hydrology: a review. *Appl Soft Comput* 19:372–386. doi:[10.1016/j.asoc.2014.02.002](https://doi.org/10.1016/j.asoc.2014.02.002)
- Rajeevan M, Bhate J, Kale JD, Lal B (2006) High resolution daily gridded rainfall data for the Indian region: analysis of break and active monsoon spells. *Curr Sci* 91(3):296–306
- Rogers JC (2013) The 20th century cooling trend over the southeastern United States. *Clim Dyn* 40(1–2):341–352
- Saji NH, Goswami BN, Vinayachandran PN, Yamagata T (1999) A dipole mode in the tropical Indian Ocean. *Nature* 401:360–363
- Samsudin R, Saad P, Shabri A (2011) River flow time series using least squares support vector machines. *Hydrol Earth Syst Sci* 15:1835–1852. doi:[10.5194/hess-15-1835-2011](https://doi.org/10.5194/hess-15-1835-2011)
- She N, Basketfield D (2005) Long range forecast of streamflow using support vector machine. In: Walton R (ed) *Proceedings of the world water and environment resources congress ASCE*, 15–19 May 2005, Anchorage: Alaska, USA. doi:[10.1061/40792\(173\)481](https://doi.org/10.1061/40792(173)481)
- Singhtrattna N, Babel MS, Perret SR (2012) Hydroclimate variability and long-lead forecasting of rainfall over Thailand by large-scale atmospheric variables. *Hydrol Sci J* 57(1):26–41
- Terray P, Delecluse P, Labattu S, Terray L (2003) Sea surface temperature associations with the late Indian summer monsoon. *Clim Dyn*. doi:[10.1007/s00382-003-0354-0](https://doi.org/10.1007/s00382-003-0354-0)
- Ting M, Kushnir Y, Seager R, Li C (2011) Robust features of Atlantic multi-decadal variability and its climate impacts. *Geophys Res Lett* 38:L17705. doi:[10.1029/2011GL048712](https://doi.org/10.1029/2011GL048712)
- Tripathi SH, Srinivas VV, Nanjundiah RS (2006) Downscaling of precipitation for climate change scenarios: a support vector machine approach. *J Hydrol* 330:621–640
- Viswambharan N, Mohanakumar K (2014) Modulation of Indian summer monsoon through northern and southern hemispheric extra-tropical oscillations. *Clim Dyn*. doi:[10.1007/s00382-014-2049-0](https://doi.org/10.1007/s00382-014-2049-0) (Springer, Article in press)
- Wang B, Liu J, Kim H, Yim S, Xiang B (2013) Northern hemisphere summer monsoon intensified by mega-El Niño/southern oscillation and Atlantic multidecadal oscillation. *Proc Natl Acad Sci USA*. doi:[10.1073/pnas.1219405110](https://doi.org/10.1073/pnas.1219405110)
- Webster PJ, Moore A, Loschnigg J, Leban M (1999) Coupled dynamics in the Indian Ocean during 1997–1998. *Nature* 401:356–360
- Willems P (2013) Multidecadal oscillatory behaviour of rainfall extremes in Europe. *Clim Change* 120(4):931–944. doi:[10.1007/s10584-013-0837-x](https://doi.org/10.1007/s10584-013-0837-x)

- Wu R, Zhang L (2010) Biennial relationship of rainfall variability between Central America and equatorial South America. *Geophys Res Lett* 37:L08701. doi:[10.1029/2010GL042732](https://doi.org/10.1029/2010GL042732)
- Ye J-S (2014) Trend and variability of China's summer precipitation during 1955–2008. *Int J Climatol* 34:559–566. doi:[10.1002/joc.3705](https://doi.org/10.1002/joc.3705)
- Zakaria ZA, Shabri A (2012) Streamflow forecasting at ungaged sites using support vector machines. *Appl Math Sci* 6(60):3003–3014